Design of tabletop hemispherical light transmittance characterization system for small scale samples

Cho, Chun Ting; de Haas, Johan; van der Kolk, Erik

DOI
10.1016/j.atech.2025.100936

Publication date
2025

Document Version
Final published version

Published in
Smart Agricultural Technology

Smart Agricultural Technology 11 (2025) 100936

Contents lists available at ScienceDirect

Smart Agricultural Technology

journal homepage: www.journals.elsevier.com/smart-agricultural-technology

Design of tabletop hemispherical light transmittance characterization system for small scale samples

Chun-Ting Cho *, Johan de Haas, Erik van der Kolk

Luminescence Materials, Delft University of Technology, Mekelweg 15, Delft, the Netherlands

ARTICLE INFO

Keywords:
Hemispherical light transmittance
Greenhouse
Covering materials
Characterization

ABSTRACT

Greenhouse owners highly value the hemispherical light transmittance (T_{HEM}) of roofing materials because sunlight rarely projects at a perpendicular angle, especially in high-latitude regions. With growing interest in research of advanced multi-functional greenhouse roofing, a compact and efficient T_{HEM} characterization system for lab-scale samples is needed to promote research in the horticulture field. In this study, we developed a tabletop system capable of characterizing T_{HEM} of lab-scale samples with a size one-third of that required by the current characterization system. Key designing parameters, such as the beam cross-section area, port area, and port edge thickness were systematically varied to evaluate their impact on T_{HEM} characterization. The results indicated that the total port area should be limited to under 1% of the sphere surface area with minimized edge thickness since reflection from the edge area can not be corrected by a double-beam measurement. Furthermore, the collimated beam cross-section area should exceed the port area by a factor of 1.5 to ensure that T_{HEM} remains unaffected by the sphere rotation center. The system provides a consistent and reliable method for T_{HEM} measurement and offers essential guidelines for future users to construct a similar setup.

1. Introduction

To tackle food shortage issues, controlled environment agriculture, such as greenhouses, has proved to be an efficient and secure way to produce food in a limited area while enhancing resource utilization and showing a strong toughness in extreme environments [1–4]. The amount of light transmitted into a greenhouse system has a large impact on every stage of plant growth and the final crop yield. Growers often assume that 1% extra light leads to 1% additional yield [5]. Although the greenhouse industry is more and more exploiting different artificial lighting methods to control the growing stage and maximize the yield, sunlight is by far the largest and free source of photosynthetically active radiation (PAR) [6–10].

Due to the natural solar trajectory during the day, the fraction of sunshine entering greenhouse coverings under a perpendicular angle is relatively small in high-latitude areas such as the United Kingdom and the Netherlands [11]. In addition, diffuse radiation dominates the total amount of daylight, especially in winter [12]. Therefore, the hemispherical light transmittance (T_{HEM}) of a greenhouse roofing is a more important optical property compared to the perpendicular light transmittance (or direct transmittance) for greenhouse owners and glass manufacturers. In 2008, Hemming et al. proposed a method to characterize T_{HEM} of greenhouse covering materials [12]. After the publication, a protocol for experimentally determining the hemispherical light transmittance was developed by Wageningen University and Research (WUR) [13,14]. The protocol established the characterization principles, procedures, and standards for hemispherical light transmittance measurement. An experimental facility, Transvision, was constructed to measure T_{HEM} following these protocols. It features a high-power Xenon lamp to mimic the solar spectrum and a 1-meter integrating sphere to integrate all transmitted light, regardless of angle, allowing for the testing of large coated or non-coated sample plates with a minimum size of 200 cm^2 [15]. The AM1.5g solar spectrum is presented in the Appendix. Later, in 2018, this protocol was replaced by the Dutch Norm NEN-2675+C1:2018 (NEN-2675), which regulates the characterization method by the Netherlands government, providing more detailed characterization guidelines [16]. Hemming et al. characterized several conventional greenhouse roofing materials and reported the perpendicular transmittance and hemispherical light transmittance information of these materials using the Transvision system [17].

The interest in advanced greenhouse roofing with a wide range of functionalities such as solar spectral conversion [18–22], light scattering

* Corresponding author.
E-mail address: c.cho@tudelft.nl (C.T. Cho).

https://doi.org/10.1016/j.atech.2025.100936
Received 25 February 2025; Received in revised form 2 April 2025; Accepted 4 April 2025
Available online 10 April 2025

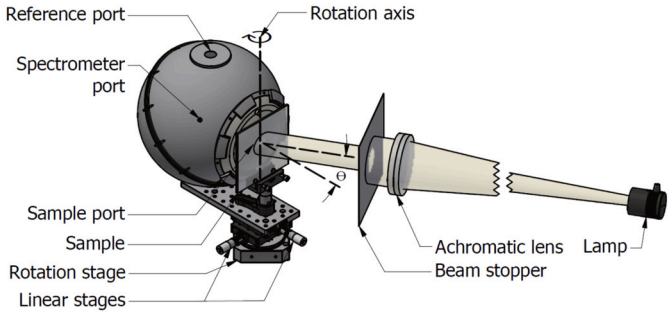

Fig. 1. Illustration of the whole tabletop hemispherical light transmittance characterization setup.

[23–26], and shading [27–30] has grown rapidly over the past decade. Nonetheless, it is challenging for research groups to build a 200 cm^2 homogeneous sample to test its T_{HEM} in the WUR Transvision system. This large-scale apparatus is accessible only to specialized laboratories, limiting public access to the resulting data and hindering broader acceptance. Therefore, there is a clear need for a tabletop T_{HEM} characterization setup suitable for lab-scale homogeneous samples smaller than 200 cm^2. However, experimental data indicates that simply scaling down optical setups introduces systematic uncertainties that were previously thought to be insignificant. Additionally, there is a lack of clear guidance on design parameters in the NEN-2675 document. For instance, the edge thickness of the integrating sphere sample port can influence the T_{HEM} value, but this issue is not addressed in NEN-2675.

In this paper, we present a tabletop hemispherical light transmittance characterization setup for a small-scale sample. We thoroughly detail its design parameters, including light beam cross-section area, integrating sphere port area and port-edge thickness, and discuss their influence on systematic uncertainties.

2. Experiments

2.1. Equipment and benchmark sample

An overview of the most important components of the proposed T_{HEM} tabletop setup can be seen in Fig. 1, which schematically shows all components that are as follows: (i) a light source (ii) an achromatic lens (iii) a beam stopper (iv) an integrating sphere with a sample port, a reference port, and a baffle inside, (v) an optical fiber connected to a spectrometer, (vi) a rotation and a linear translation stage by which the angle of incidence and the position of the rotation axis can be controlled as indicated in the figure, and finally (vii) a test sample. These components are discussed in more detail below.

(i) A powerful 150 W halogen lamp (64640 HLX, Osram) installed on a G6.35 lamp socket with a power supply was used as the light source in our setup. The lamp has a filament of 5.8 mm (width) × 2.9 mm (height). We chose a tungsten lamp instead of the xenon lamp because it has no sharp spectral features and has sufficient intensity between 400 nm and 700 nm needed for the calculation of T_{HEM}. (ii) A doublet achromatic lens (14 cm in diameter, Edmund Optics) served to collimate the light emitted from the lamp, ensuring a parallel beam necessary for accurate measurement. Due to the lamp filament not being a point source, a perfect 0° divergence cannot be achieved. For all the tests in this study, the default beam divergence was set to the minimum (~0°). (iii) The beam stopper located behind the achromatic lens served to control the beam diameter. (iv) A home-built 30 cm diameter integrating sphere allowed for easily interchanging ports with varying diameters. The interior of the sphere was coated with diffusive barium sulfate (Gigahertz-Optik). The interiors of all exchangeable ports were also coated with barium sulphate. Besides the exchangeable port, the integrating sphere has an additional port referred to as "reference port" for the double beam measurement, as explained later in more detail in section 2.2. (v) An optical fiber (FC-UVIR600-1, Avantes) connected the spectrometer port to the spectrometer (QE65Pro, Ocean Optics) to measure the light intensity captured by the integrating sphere. (vi) The rotation stage (HDR50, Thorlabs) served to automatically rotate the integrating sphere so that the incident angle of the beam could be controlled from 0° to 75°. A linear translation stage was installed to adjust the position of the rotation axis. (vii) A 4 mm thick Optiwhite (Pilkington) glass with a reported direct transmittance of 92% and hemispherical light transmittance of 84% (measured by WUR Transvision system) was used as the benchmark sample for all the measurements in this research. In our system, a beam splitter to project the light beam on the reference port is not needed. Instead, we manually rotated the whole integrating sphere by 90° to exchange the position of the sample port and the reference port.

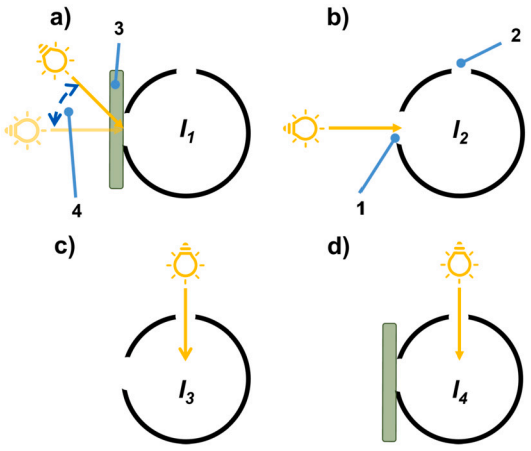

Fig. 2. Illustration of measurement steps a to d. 1: the sample port. 2: the reference port. 3: sample. 4: the angle of incidence θ.

2.2. Measurement procedure

According to NEN-2675, the transmittance measurement of samples is performed for at least eight incident angles (θ = 0°, 15°, 30°, 40°, 45°, 50°, 60°, and 75°), with each measurement referred to as an angular-spectral transmittance ($T_{\lambda,\theta,\phi}$) for a fixed azimuthal angle ϕ (in standard spherical coordinates) and a wavelength range between 400 nm and 700 nm [16]. The transmittance of a material is defined as the ratio of the transmitted light intensity (Fig. 2a) to the incident light intensity (Fig. 2b). The latter is recorded without a sample and is referred to as the reference or lamp measurement. The transmittance measurement performed with an integrating sphere usually overestimates the transmittance. This is because a fraction of the light that enters the integrating sphere (in the reference measurement without a sample) exits the sphere through the sample port after many diffuse reflections within the sphere. This fraction is, however, not the same when a sample is present due to the reflections at the sample surface that do not occur without the sample located in front of the measuring port. This difference can be quantified and thereby corrected through a so-called double-beam measurement (Fig. 2c and d) as described in the NEN-13468-2-2021 document [31]. The measurement steps for a comprehensive T_{HEM} characterization are described below and shown in Fig. 2.

(a) Sample port is illuminated with sample in the sample port. The measured light intensity is $I_{\lambda,\theta,\phi,1}$.
(b) Sample port is illuminated without sample in the sample port. The measured light intensity is $I_{\lambda,\theta,\phi,2}$.
(c) Reference port is illuminated without sample in the sample port. The measured light intensity signal is $I_{\lambda,\theta,\phi,3}$.
(d) Reference port is illuminated with sample in the sample port. The measured light intensity is $I_{\lambda,\theta,\phi,4}$.

All measured light intensities are corrected to exclude dark noise from the background. Based on measurements (a) through (d), the corrected angular-spectral transmittance $T_{\lambda,\theta,\phi}$ is as below:

$$T_{\lambda,\theta,\phi} = \frac{I_{\lambda,\theta,\phi,1}}{I_{\lambda,\theta,\phi,2}} \times \frac{I_{\lambda,\theta,\phi,3}}{I_{\lambda,\theta,\phi,4}} \quad (1)$$

The term $I_{\lambda,\theta,\phi,3}/I_{\lambda,\theta,\phi,4}$ is referred to as the double-beam coefficient which corrects for the over-estimated transmittance described above.

Note that the double-beam coefficient strongly depends on the probability that light scattered around within the integrating sphere exits the sphere through the sample port. A larger port represents a larger probability of light escaping. This probability is independent of where light first hits the integrating sphere after entering through the sample port. However, we hypothesize that this probability is much higher for light that strikes the edge of the sample port after entering through the sample port, potentially reaching an escape probability as high as 50%, which is much higher than that of light hitting the sphere's inner surface after entering through the sample port. We will show that, indeed, these so-called edge thickness effects are not corrected for by a double-beam experiment and, therefore, must be minimized.

2.3. Calculation of hemispherical light transmittance T_{HEM}

The hemispherical light transmittance T_{HEM} is calculated by the angle-dependent transmittance $T_{\theta,\phi}$ through numerical integration over the wavelength of the previously described angular-spectral transmittance $T_{\lambda,\theta,\phi}$:

$$T_{\theta,\phi} = \frac{\int_{400}^{700} A_\lambda \times T_{\lambda,\theta,\phi} d\lambda}{\int_{400}^{700} A_\lambda d\lambda} = 0.00045 \times \int_{400}^{700} A_\lambda \times T_{\lambda,\theta,\phi} d\lambda \quad (2)$$

Where A_λ is the product of the relative spectral density of solar radiation and relative plant sensitivity function in the PAR range that is defined by the NEN-2675. The hemispherical light transmittance T_{HEM} is calculated from the angle-dependent transmittance $T_{\theta,\phi}$ according to the equation:

$$T_{HEM} = \frac{\int_0^{2\pi} \int_0^{\pi/2} T_{\theta,\phi} \times S_{\theta,\phi} \times sin(\theta) \times cos(\theta) d\theta d\phi}{\int_0^{2\pi} \int_0^{\pi/2} S_{\theta,\phi} \times sin(\theta) \times cos(\theta) d\theta d\phi} \quad (3)$$

In this formula, ϕ represents an azimuthal angle (in standard spherical coordinates) and $S_{\theta,\phi}$ represents a solar luminance distribution function. We assume the "standard uniform sky" (for which $S = 1$) is applied. It can be defined otherwise in case luminance distribution changes with latitude and azimuth. Note that the azimuthal angle ϕ is not relevant in our study due to the glass sample used being homogeneous without anisotropic surface modification. In the case of an inhomogeneous sample, measurements need to be taken at different azimuthal angles ϕ as defined in NEN-2675.

2.4. Beam profile

The beam profile of the light source was measured using an optical fiber (FC-UVIR600, Avantes) connected to a spectrometer (QE65Pro, Ocean Optics). The inlet of the optical fiber faced the light source, and its position was controlled by an automated linear translation stage (DDS100, Thorlabs) moving horizontally across the centerline of the beam to measure the profile.

2.5. Design parameters

To determine the required dimensions of our tabletop T_{HEM} characterization system, several design parameters were tested to establish that T_{HEM} remains independent within a certain range of specific parameters indicating the absence of systematic uncertainties. These parameters are discussed below. Note that NEN-2675 implicitly suggests the rotation center of the integrating sphere (as shown by the rotation axis in Fig. 1) should align with the sample port plane. We performed a simple test to determine the position of the rotation center, which shows no difference when applying a highly collimated light beam that is larger than the port area as demonstrated in the Appendix.

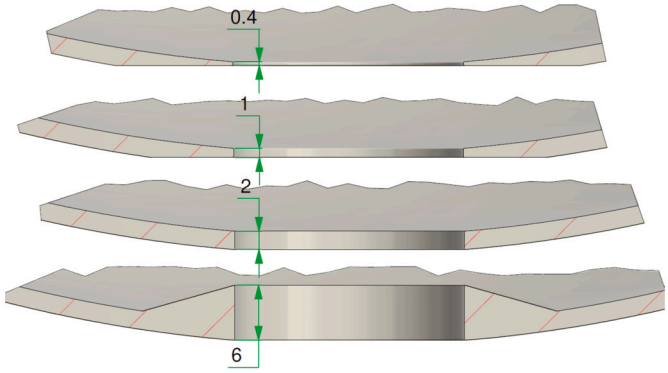

Fig. 3. Illustration of the sample port edge with different thickness, 0.4, 1, 2, 6 mm on a 25 mm diameter port.

2.5.1. Port-to-sphere surface area ratio

The port area introduces a systematic error, resulting in an overestimation of T_{HEM}, as explained in section 2.2. This error can be corrected by using the double-beam coefficient. The goal of this section is to validate the correction function of the double-beam coefficient. Three interchangeable ports with different diameters (25, 50, and 100 mm) were produced. The ratios of the total port area to the total sphere surface area (referred to as the "port-to-sphere surface area ratio") are 0.35%, 0.87%, and 2.95%, respectively.

2.5.2. Port edge thickness

Prior to this study, we observed that the "edge thickness" of the sample port, as illustrated in Fig. 3, influenced the T_{HEM} value. When a light beam with a high angle of incidence (large value for θ strikes the integrating sphere with a thick edge, a large fraction of light first undergoes a Lambertian reflection at the edge area before reaching the inner sphere surface. Due to the location of the edge area being very close to the port opening, approximately half of the reflected light (assuming an ideal Lambertian scattering surface) escapes through the port when no sample is present. In contrast, when light first hits the sphere's inner surface rather than the edge area, the probability of it leaving the port is proportional to the ratio of the port area to the total sphere inner surface area, which is in the order of a few % [32]. This phenomenon introduces uncertainties in T_{HEM} calculation, which grow larger when the edge area increases, as further explained in Fig. 4.

To investigate the impact of port edge thickness on the T_{HEM} value, four interchangeable ports (the sample port in Fig. 1) with varying edge thicknesses (0.4, 1, 2, and 6 mm) and a fixed port diameter of 25 mm were produced. The design details are provided in Fig. 3. The reference port has a diameter of 25 mm and an edge thickness of 0.4 mm.

2.5.3. Beam-to-port area ratio

The direction of light propagation changes upon entering a medium with a different refractive index, such as from air ($n = 1$) to glass ($n = 1.5$), due to refraction. The refraction within the glass results in a lateral shift in the light path [33]. In addition, the circular illumination area (referred to as "beam cross-section area") of a collimated incident beam (at $\theta = 0^\circ$) expands into an elliptical shape at higher angles of incidence. The semi-major axis length of the ellipse is inversely proportional to $\cos(\theta)$, while the semi-minor axis remains the same as the radius of the original beam. Based on the area equations for an ellipse and a circle, the area of the expanded ellipse follows an inverse relationship with $\cos(\theta)$

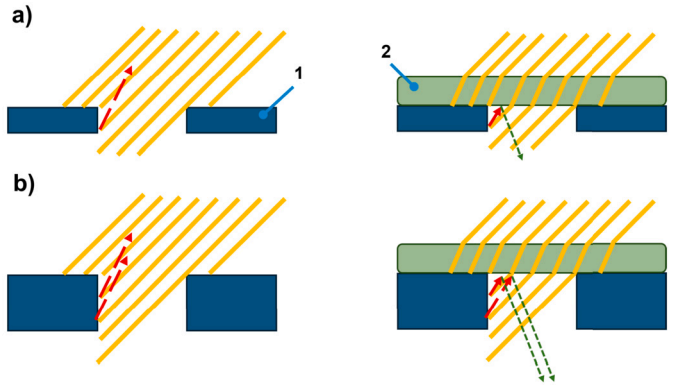

Fig. 4. Illustration of edge reflection on ports. 1: port edge. 2: sample. a) Small edge thickness. b) Large edge thickness. At large angles of incidence θ, a large fraction of light hits the port edge instead of entering the sphere. Red arrows represent light reflected from the edge area while green arrows represent light reflected back from the sample into the sphere.

as A' = A/cos(θ), where A is the original circular illuminating area of the beam when the incident angle is 0°, and A' is the expanded illuminating area at a given incident angle. This area-expansion effect, combined with the aforementioned lateral shift in light, impacts the T_{HEM} to an extent depending on the area ratio between the beam and the port, which is referred to as "beam-to-port area ratio".

When applying a beam with a beam cross-section area that is approximately the same size as the port area, a systematic error can occur. This is because the fractions of light entering the sphere with and without the sample differ due to the lateral shift effect discussed previously, which means some portions of the light can be blocked by the sphere wall, as shown in Fig. 5a. Utilizing a collimated light beam with a cross-section area that is sufficiently larger than the port area can minimize this problem since the fraction of light after the lateral shift is the same with and without a sample as shown in Fig. 5b. This is also discussed in the NEN-2675 document, stating that: the illuminating area should be at least 15% larger than the size of the sample port.

Swinkels discussed the possibility of using a beam that is much smaller than the port area [15]. The issue of the sphere receiving different fractions of light could be potentially minimized if all the light exiting the glass sample were collected by the integrating sphere; in other words, no light is blocked by the sphere wall, as shown in Fig. 5c. In the results, we show that this might be true but only when the divergence of the beam is sufficiently small (~0°).

To determine the required beam-to-port area ratio for our tabletop characterization system, we applied different-sized beam stoppers to adjust the beam cross-section area and tested these beams with ports of varying diameters. This allowed us to evaluate the combined influence of beam cross-section area and port area on the T_{HEM} value. The ratio of the beam cross-section area to the port area, referred to as "beam-to-port area ratio", serves to be a practical parameter for future users designing setups to accurately measure T_{HEM}.

3. Results and discussions

3.1. The influence of port-to-sphere surface area ratio

To ensure a fair comparison of the influence of varying port areas, the measurements were conducted at a beam-to-port area ratio of 144% for the three ports with a small port edge thickness of 0.4 mm. The significance of the double-beam coefficient in T_{HEM} characterization is illustrated in Fig. 6, which compares T_{HEM} values with and without applying the double-beam coefficient.

When applying the double-beam coefficient, the T_{HEM} values decreased only slightly from 85.5% to 85.1% as the port area increased, remaining within the ±1% acceptance range defined by NEN-2675. In contrast, the T_{HEM} without applying a double-beam coefficient ($I_{\lambda,\theta,\phi,3}/I_{\lambda,\theta,\phi,4} = 1$ in equation) increased from 86.2% to 91.4%. The result indicated that the double-beam coefficient effectively corrects the overestimation of T_{HEM}.

The influence of applying the double-beam coefficient was quantified by the term "double-beam factor (DBF)", which is a wavelength- and angular-integrated double-beam coefficient derived from Eq. (1) by setting $I_{\lambda,\theta,\phi,1}/I_{\lambda,\theta,\phi,2} = 1$. The DBF indicates the extent of correction conducted by the double-beam measurement: a DBF of 1 means no correction, while smaller DBF values indicate a greater extent of correction. Due to equipment limitations, a further increase in the port area was not feasible in this study. However, the result demonstrated a trend of T_{HEM} following NEN-2675 regulation, which states that the total port area should not exceed 3% of the total sphere surface area. To preserve the functionality of the integrating sphere with a minimal correction factor, we recommend keeping the total port area below 1% of the total sphere surface area. Note that the double-beam coefficient for the three ports with different diameters is independent of the angle of incidence (θ) as demonstrated in the Appendix.

3.2. The influence of port edge thickness

In section 2.5.2, we explained that light directly hitting the edge of the sample port introduces a systematic error in T_{HEM} that cannot be corrected by a double-beam factor. Therefore, we expected the systematic error to increase with the edge thickness. To evaluate this, a 40 mm beam was applied to 25 mm ports, each with different edge thicknesses (0.4, 1, 2, 6 mm).

As shown in Fig. 7, T_{HEM} increases from 85.5% to 88.5% (blue curve, with double-beam correction) and from 86.1% to 89.0% (red curve, without double-beam correction) when the edge thickness increases from 0.4 mm to 6 mm. The result demonstrated that the double-beam coefficient could not correct the T_{HEM} for different edge thicknesses as in Fig. 6. This is confirmed by the green curve in Fig. 7, which shows just a minor change in the DBF value when varying the edge thickness from 0.4 mm to 6 mm showing that the DBF is independent of the edge thickness.

A deeper understanding of the influence of the edge thickness on T_{HEM} is presented in Fig. 8. The angular transmittance of the ports with the thinnest edge (0.4 and 1 mm) shows a decrease with increasing incident angles as predicted by Fresnel's equations, as illustrated by the red curve in Fig. 8b. A similar result was obtained by Hemming et al. [34]. However, the angular transmittance for the 2 mm and 6 mm port edge thicknesses shows an increase in transmittance as a function of the angle between $\theta = 30°$ and 50° compared to $\theta = 0°$, which contradicts Fresnel's equations. The observed higher transmission for larger angles can only be explained by the effect of the increased edge surface, as discussed previously. Based on this observation, we recommend designing the port edges as thin as possible, in this study, less than 1 mm for a 25 mm port. This edge effect is negligible for the WUR Transvision system since the port diameter of the Transvision system is large (170 mm) compared to the thickness of the integrating sphere edge (which can be up to 10 mm). While we acknowledge that additional experiments, particularly those systematically varying port-edge thickness across a broader range of port diameters, could further reinforce our findings, the current results provide sufficient guidance for designing a down-scaled system.

3.3. The influence of beam-to-port area ratio

In this section, we present the results of the beam-to-port area ratio test conducted on three different sizes of ports (25 mm, 50 mm, and 100 mm) with an edge thickness of 0.4 mm. Fig. 9 illustrates the T_{HEM} as a function of the beam-to-port area ratio for the three ports. The T_{HEM} values for 25 mm and 50 mm ports remained stable when the beam cross-section area exceeded the port area by a factor of 1.5 (150% beam-to-port area ratio). However, when the T_{HEM} was measured with a

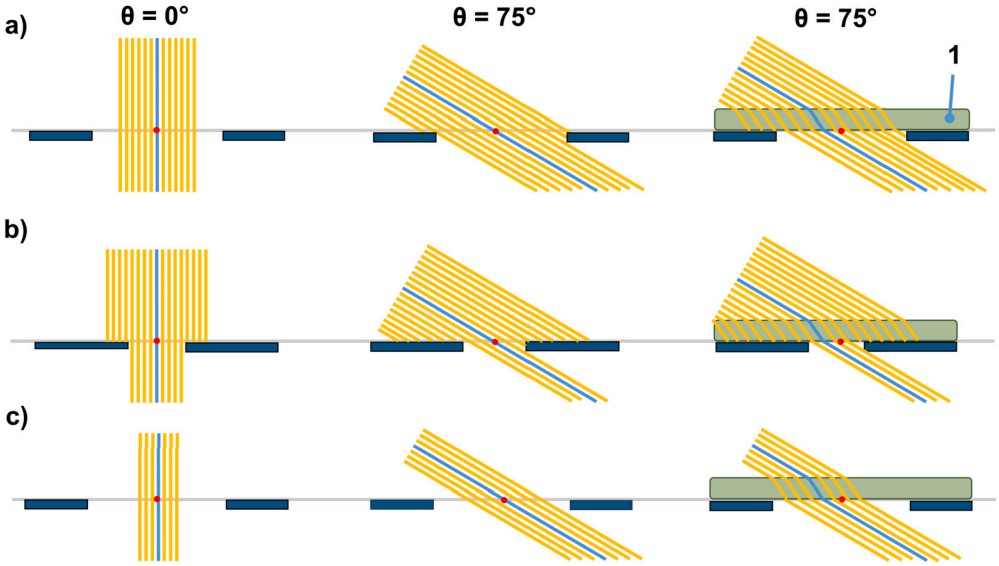

Fig. 5. Illustration of conditions of different beam cross-section area to port area at 0° and 75° angle of incidence. 1: sample. a) Beam cross-section area is smaller than the port. b) Beam cross section area is much larger than the port. c) Beam cross-section area is much smaller than the port.

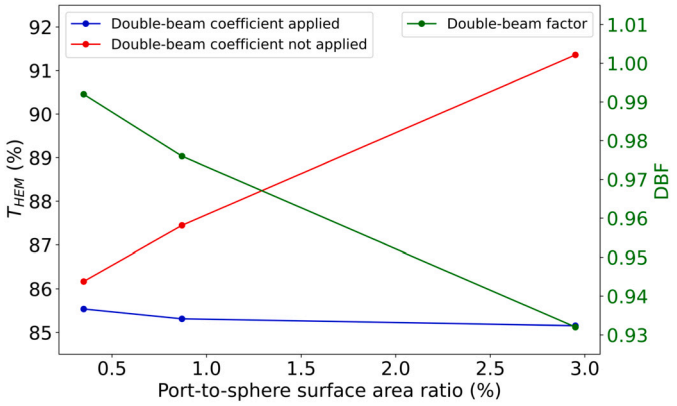

Fig. 6. The T_{HEM} of the 25 mm, 50 mm, and 100 mm ports with and without the correction of double-beam coefficient, and the double-beam factor (DBF). The ratio of total port area to sphere surface area for 25 mm, 50 mm, and 100 mm ports are 0.35%, 0.87%, and 2.95%, respectively. All the ports have an edge thickness of 0.4 mm. The applied beam-to-port area ratio is 144%.

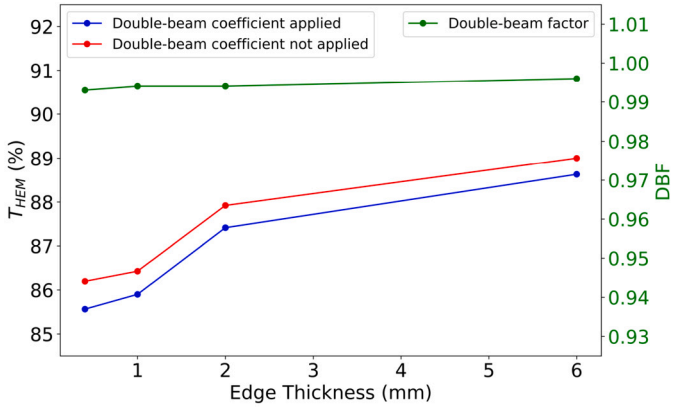

Fig. 7. The T_{HEM} of 25 mm ports with edge thickness 0.4, 1, 2, and 6 mm ports with and without the correction of double-beam coefficient, and the double-beam factor (DBF). A 40 mm beam was applied to the ports.

smaller beam-to-port area ratio (<150%), the results showed a decreasing trend due to some fractions of the light being blocked by the sphere wall, as discussed in section 2.5.3. Specifically for the 25 mm port, the result of the 4% beam-to-port area ratio beam gave a 5.5% difference in T_{HEM} compared to the T_{HEM} above 150% beam-to-port area ratio, while the other two ports gave only a difference of about 1-1,5% as can be seen in Fig. 9b.

The fact that there is a difference, and more generally, that the T_{HEM} value at small ratios is not the same as the value measured at large ratios, is attributed to the light beam not being perfectly collimated and lacking a block-shaped beam profile. This shortcoming is more pronounced for beams with smaller diameters. The beam profile deviating from a perfect block-shape is illustrated by the yellow area in Fig. 10. Especially for smaller diameter beams, the low-intensity illuminating ring (blue area) surrounding the uniform block-shaped beam (yellow area) is relatively large. As shown in Fig. 10, light passing through a 5 mm beam stopper contains a larger fraction of the imperfect illuminating region compared to the central collimated area than light passing through a 10 mm beam stopper. According to Snell's law, a 75° incident angle refracts to 40° inside the glass, while the critical angle for total internal reflection (TIR) from air (n = 1) to Optiwhite glass (n = 1.5) is 41.9°. We believe that the imperfect illuminating region contains non-collimated beams that exceed the TIR angle after refraction in the glass, leading to reduced transmittance at $\theta = 75°$ for the 25 mm port compared to the larger ports with the same beam-to-port area ratio (Fig. 11), resulting in the great difference in the T_{HEM} values. Additionally, we note that multiple reflections at such large angles of incidence might lead to the reduced transmittance if part of the beam undergoes higher-order reflections in the 25 mm port. However, this alone cannot fully explain why no difference was observed in the larger ports (Fig. 11b).

Based on the observation, the concept of using a beam much smaller than the port area, with a sufficiently low beam divergence, may be feasible for achieving the same T_{HEM} as applying a beam that is 50% larger than the port area. However, achieving such low divergence is particularly challenging when working with small beam diameters and basic optical components, such as the extended light source used in our study. The result indicated that the beam cross-section area should exceed the port area (over 150%) to obtain a steady result in this study. Based on this observation, we recommend applying a beam with the cross-section area being at least 50% larger than the port area for a stable result.

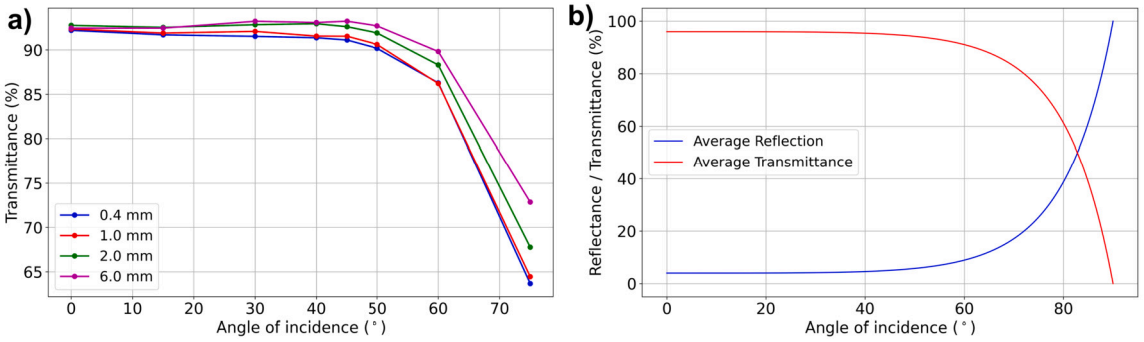

Fig. 8. a) The angular transmittance of 25 mm ports with edge thickness 0.4, 1, 2, and 6 mm ports. b) The transmittance and reflectance of light entering the air (n = 1) from Optiwhite (n = 1.5) based on Fresnel equations.

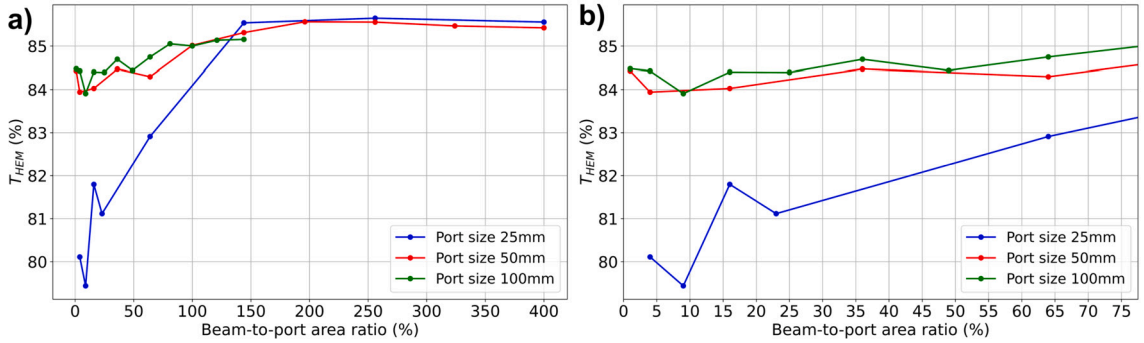

Fig. 9. a) The T_{HEM} of various beam-to-port area ratios on the exchangeable ports of 25 mm, 50 mm, 100 mm. b) The zoom-in of a). All the ports have an edge thickness of 0.4 mm.

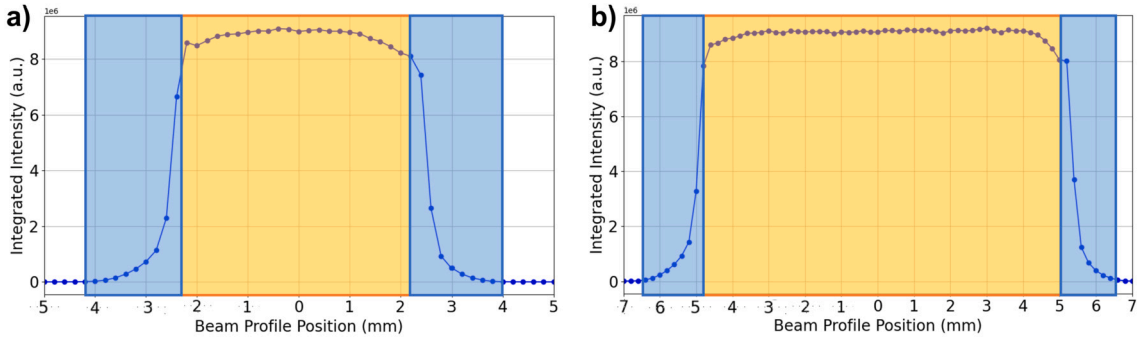

Fig. 10. The beam profile of a) light passing through a 5 mm beam stopper and b) light passing through a 10 mm beam stopper. The central part of beam with homogeneous light intensity is marked with yellow color. The imperfect illuminating region of the beam is marked with blue color.

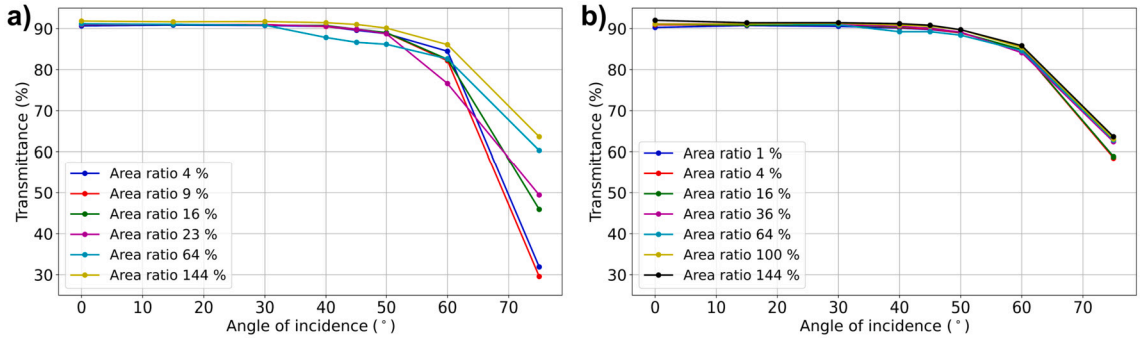

Fig. 11. The angular transmittance of different beam-to-port area ratio of a) 25 mm port. b) 50 mm port.

Table 1
Comparison of angular transmittance, standard deviation, and T_{HEM} of Optiwhite glass characterized by WUR Transvision system and by our setup.

Angle of incidence (θ)	0°	15°	30°	40°	45°	50°	60°	75°	T_{HEM}
	WUR Transvision								
Transmittance (%)	91.61	91.57	91.29	90.52	89.92	88.97	84.04	61.03	84.32
Std. (%)	0.045	0.058	0.087	0.029	0.078	0.013	0.041	0.043	0.008
	This work								
Transmittance (%)	92.11	91.72	91.69	91.37	90.89	90.02	85.96	63.61	85.49
Std. (%)	0.068	0.049	0.073	0.086	0.088	0.081	0.134	0.120	0.05

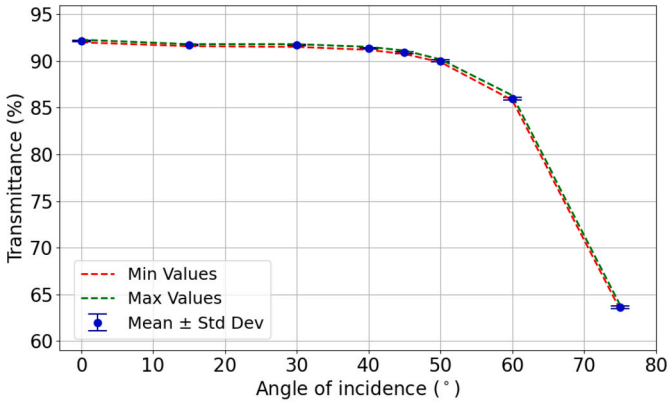

Fig. 12. The angular transmittance and standard deviation analysis of 20 tests on the Optiwhite sample using the optimal parameters.

3.4. Repeatability test

Based on the results of the tests above, we determined the optimal parameters for our desktop system and conducted a repeatability test. The applied parameters were the 25 mm diameter port with 0.4 mm thickness, a 40 mm diameter beam with ~0° beam divergence, and the rotation center aligned with the same plane as the sample port. Table 1 shows the angular transmittance of 4 mm Optiwhite characterized by WUR Tansvision system and by our system based on a 20x repeatability test of removing and repositioning the sample. Fig. 12 shows the standard deviation result of our test. The standard deviation of our setup is comparable to that of WUR Transvision system. Our results demonstrated that the spread in T_{HEM} is within ±1%, which falls within the acceptable range regulated by NEN-2675.

3.5. Required sample dimension

Based on the area-expansion equation mentioned in section 2.5.3, the semi-major axis of the expanded ellipse becomes 3.86 times the original radius of the incident beam at a 75° angle of incidence and the semi-minor axis of the ellipse remains unchanged at the original beam radius. For a 40 mm incident beam, the minimum required length of the sample is four times the diameter (160 mm), while the minimum width can be 45 mm which is slightly larger than the beam diameter to be illuminated by the full incident beam. Thus, the minimum required sample is one-third (72 cm^2) of the required dimension of the WUR Transvision system. A smaller sample dimension can be achieved if a smaller beam is used. It is important to note that the target samples characterized by this setup should be homogeneous and free of distinct repeating patterns.

4. Conclusion

A compact, tabletop system has been successfully developed to characterize the hemispherical light transmittance (T_{HEM}) of lab-scale samples. A commercial product with known T_{HEM} was used to benchmark the influence of these design parameters. Key findings indicated that the port edge thickness should be minimized to reduce edge reflection effects, and the port area should be kept below 1% of the total sphere surface area to ensure accurate measurements. Furthermore, the applied beam cross-section area should exceed the port area by at least 150% to maintain measurement stability. Results further highlight the importance of maintaining a low beam divergence (close to 0°) and aligning the rotation center with the plane of the sample port to minimize potential discrepancies, particularly for small beam diameters. The minimum required sample length should be four times the applied beam cross-section area, while the width should be sufficient to ensure a full beam illumination. These findings provide essential design guidelines for building customized tabletop characterization systems, enabling research groups to characterize small-scale samples efficiently and reproducibly.

By making T_{HEM} characterization more accessible to research groups, this system can accelerate the development of advanced optical coatings. In the long run, such innovations can be transferred to commercial greenhouse roofing products, benefiting greenhouse farmers through improved light management and potentially higher crop yields.

CRediT authorship contribution statement

Chun-Ting Cho: Writing – original draft, Visualization, Validation, Methodology, Investigation, Formal analysis, Conceptualization. **Johan de Haas:** Software, Methodology, Conceptualization. **Erik van der Kolk:** Writing – review & editing, Supervision, Project administration, Methodology, Funding acquisition, Conceptualization.

Declaration of generative AI and AI-assisted technologies in the writing process

During the preparation of this work, the author(s) used Chatgpt in order to enhance the readability. After using this tool/service, the author(s) reviewed and edited the content as needed and take(s) full responsibility for the content of the published article.

Funding

This research received funding from the Dutch Research Council (NWO) in the framework of the Science PPP Fund for the top sectors and from the Ministry of Economic Affairs in the framework of the “PPS-Toeslagregeling”.

Declaration of competing interest

The authors declare that they have no known competing financial interests or personal relationships that could have appeared to influence the work reported in this paper.

Acknowledgement

The authors thank Dr. Giacomo Bosco (Fotoniq B.V.) for his helpful comments.

Appendix A. Supplementary material

Supplementary material related to this article can be found online at https://doi.org/10.1016/j.atech.2025.100936.

Data availability

Data will be made available on request.

References

[1] D. Zhou, H. Meinke, M. Wilson, L.F. Marcelis, E. Heuvelink, Towards delivering on the sustainable development goals in greenhouse production systems, Resour. Conserv. Recycl. 169 (2021), https://doi.org/10.1016/j.resconrec.2020.105379.

[2] P. Zabel, M. Bamsey, D. Schubert, M. Tajmar, Review and analysis of over 40 years of space plant growth systems, Life Sci. Space Res. 10 (2016) 1–16, https://doi.org/10.1016/j.lssr.2016.06.004.

[3] C. Maraveas, Environmental sustainability of greenhouse covering materials, Sustainability (Switzerland) 11 (21) (2019), https://doi.org/10.3390/su11216129.

[4] R.W.J. Giacomelli, A. Gene, Greenhouse Covering Systems, HortTechnology, 1993.

[5] L.F. Marcelis, A.G. Broekhuijsen, E. Meinen, E.M. Nijs, M.G. Raaphorst, Quantification of the growth response to light quantity of greenhouse grown crops, Acta Hortic. 711 (2006) 97–103, https://doi.org/10.17660/actahortic.2006.711.9.

[6] M.A. Jones, Using light to improve commercial value, Hortic. Res. 5 (1) (2018), https://doi.org/10.1038/s41438-018-0049-7.

[7] J.A. Nelson, B. Bugbee, Economic analysis of greenhouse lighting: light emitting diodes vs. high intensity discharge fixtures, PLoS ONE 9 (6) (2014), https://doi.org/10.1371/journal.pone.0099010.

[8] E. Kaiser, T. Ouzounis, H. Giday, R. Schipper, E. Heuvelink, L.F. Marcelis, Adding blue to red supplemental light increases biomass and yield of greenhouse-grown tomatoes, but only to an optimum, Front. Plant Sci. 9 (January 2019) 1–11, https://doi.org/10.3389/fpls.2018.02002.

[9] C. Gómez, R.C. Morrow, C.M. Bourget, G.D. Massa, C.A. Mitchell, Comparison of intracanopy light-emitting diode towers and overhead high-pressure sodium lamps for supplemental lighting of greenhouse-grown tomatoes, HortTechnology 23 (1) (2013) 93–98, https://doi.org/10.21273/horttech.23.1.93.

[10] S. Hemming, Use of natural and artificial light in horticulture - interaction of plant and technology, Acta Hortic. 907 (2011) 25–35, https://doi.org/10.17660/ActaHortic.2011.907.1.

[11] P. Rajendran, H. Smith, Modelling of solar irradiance and daylight duration for solar-powered UAV sizing, Energy Explor. Exploit. 34 (2) (2016) 235–243, https://doi.org/10.1177/0144598716629874.

[12] S. Hemming, V. Mohammadkhani, T. Dueck, Diffuse greenhouse covering materials - material technology, measurements and evaluation of optical properties, Acta Hortic. 797 (2008) 469–476, https://doi.org/10.17660/actahortic.2008.797.68.

[13] J. Ruigrok, G.-J. Swinkels, Lichtmeetprotocol Kasdekmaterialen Samenvatting, 2010, p. 27.

[14] G.-J. Swinkels, S. Hemming, V. Mohammadkhani, J. Van Ruijven, Rapport GTB-1252 Protocol for measuring light transmission of horticultural screens, www.greenhousehorticulture.wur.nl, 2012.

[15] G.L. Swinkels, Transvision: a light transmission measurement system for greenhouse covering materials, Acta Hortic. 956 (2012) 563–568, https://doi.org/10.17660/ActaHortic.2012.956.67.

[16] K.N. Normalisatie-instituut, NEN 2675+C1 Greenhouse glass - Determination of optical properties of greenhouse covering materials and screens, Tech. Rep., 2018.

[17] S. Hemming, G.L. Swinkels, A.J. Van Breugel, V. Mohammadkhani, Evaluation of diffusing properties of greenhouse covering materials, Acta Hortic. 1134 (2016) 309–316, https://doi.org/10.17660/ActaHortic.2016.1134.41.

[18] C. Cho, G. Bosco, E. van der Kolk, The potential of $SiO_2 : Al^{3+}$, Eu^{2+} blue phosphor coatings in greenhouse application, Opt. Mater. 157 (2024) 2–8.

[19] K. Mishra, C. Stanghellini, S. Hemming, Technology and materials for passive manipulation of the solar spectrum in greenhouses, Adv. Sustain. Syst. 7 (5) (2023), https://doi.org/10.1002/adsu.202200503.

[20] S.K. Jakka, M.M. Silva, M.J. Soares, K. Pavani, Exploring the potential of Eu3+ and Mn4+ activated LaAlO3 phosphors as red and far-red emitters for horticulture lighting, RSC Adv. 13 (45) (2023) 31314–31320, https://doi.org/10.1039/d3ra03241h.

[21] C.H. Parrish, D. Hebert, A. Jackson, K. Ramasamy, H. McDaniel, G.A. Giacomelli, M.R. Bergren, Optimizing spectral quality with quantum dots to enhance crop yield in controlled environments, Commun. Biol. 4 (1) (2021) 1–9, https://doi.org/10.1038/s42003-020-01646-1.

[22] R.A. Yalçın, H. Ertürk, Improving crop production in solar illuminated vertical farms using fluorescence coatings, Biosyst. Eng. 193 (2006) (2020) 25–36, https://doi.org/10.1016/j.biosystemseng.2020.02.007.

[23] S. Hemming, T. Dueck, J. Janse, F. Van Noort, The effect of diffuse light on crops, Acta Hortic. 80 (1 PART 2) (2008) 1293–1300, https://doi.org/10.17660/ActaHortic.2008.801.158.

[24] F.L. Kempkes, C. Stanghellini, N.G. Victoria, M. Bruins, Effect of diffuse glass on climate and plant environment: first results from an experiment on roses, Acta Hortic. 952 (2012) 255–262, https://doi.org/10.17660/ActaHortic.2012.952.31.

[25] T. Dueck, J. Janse, T. Li, F. Kempkes, B. Eveleens, Influence of diffuse glass on the growth and production of tomato, Acta Hortic. 956 (2012) 75–82, https://doi.org/10.17660/ActaHortic.2012.956.6.

[26] R.A. Yalçin, H. Ertürk, Improving photosynthetic efficiency using greenhouse coatings with scattering and fluorescent pigments, Mater. Res. Express 6 (8) (2019), https://doi.org/10.1088/2053-1591/ab28b8.

[27] A. Baille, C. Kittas, N. Katsoulas, Influence of whitening on greenhouse microclimate and crop energy partitioning, Agric. For. Meteorol. 107 (4) (2001) 293–306, https://doi.org/10.1016/S0168-1923(01)00216-7.

[28] H.A. Aldaftari, J. Okajima, A. Komiya, S. Maruyama, Radiative control through greenhouse covering materials using pigmented coatings, J. Quant. Spectrosc. Radiat. Transf. 231 (2019) 29–36, https://doi.org/10.1016/j.jqsrt.2019.04.009.

[29] T. Li, Y. Gao, K. Zheng, Y. Ma, D. Ding, H. Zhang, Achieving better greenhouse effect than glass: visibly transparent and low emissivity metal-polymer hybrid metamaterials, ES Energy Environ. 5 (2019) 102–107, https://doi.org/10.30919/esee8c325.

[30] H. Gonome, M. Baneshi, J. Okajima, A. Komiya, S. Maruyama, Controlling the radiative properties of cool black-color coatings pigmented with CuO submicron particles, J. Quant. Spectrosc. Radiat. Transf. 132 (2014) 90–98, https://doi.org/10.1016/j.jqsrt.2013.02.027.

[31] K.N. Normalisatie-instituut, NEN-EN-ISO 13468-2 Plastics - Determination of the total luminous transmittance of transparent materials - Part 2: Double-beam instrument (ISO 13468-2:2021, IDT), 2021.

[32] Labsphere, Integrating Sphere Radiometry and Photometry Technical Guide, PB-16010-000 Rev.00, 2017.

[33] J.C. Jonsson, G.B. Smith, C. Deller, A. Roos, Directional and angle-resolved optical scattering of high-performance translucent polymer sheets for energy-efficient lighting and skylights, Appl. Opt. 44 (14) (2005) 2745–2753, https://doi.org/10.1364/AO.44.002745.

[34] S. Hemming, V. Mohammadkhani, J. Van Ruijven, Material technology of diffuse greenhouse covering materials - influence on light transmission, light scattering and light spectrum, Acta Hortic. 1037 (2014) 883–896, https://doi.org/10.17660/actahortic.2014.1037.118.